

## Article

# Synthesis of Visible-Light Driven CrxOy-TiO<sub>2</sub> Binary Photocatalyst System Based on Hierarchical Macro-Mesoporous Silica

Sen, Tapas

Available at <http://clock.uclan.ac.uk/13711/>

*Sen, Tapas ORCID: 0000-0002-0463-7485 (2014) Synthesis of Visible-Light Driven CrxOy-TiO<sub>2</sub> Binary Photocatalyst System Based on Hierarchical Macro-Mesoporous Silica. Applied Catalysis B: Environmental, 163 . pp. 9-15. ISSN 0926-3373*

It is advisable to refer to the publisher's version if you intend to cite from the work.  
<http://dx.doi.org/10.1016/j.apcatb.2014.06.024>

For more information about UCLan's research in this area go to  
<http://www.uclan.ac.uk/researchgroups/> and search for <name of research Group>.

For information about Research generally at UCLan please go to  
<http://www.uclan.ac.uk/research/>

All outputs in CLoK are protected by Intellectual Property Rights law, including Copyright law. Copyright, IPR and Moral Rights for the works on this site are retained by the individual authors and/or other copyright owners. Terms and conditions for use of this material are defined in the [policies](#) page.

# Synthesis of Visible-Light Driven $\text{Cr}_x\text{O}_y\text{-TiO}_2$ Binary Photocatalyst System Based on Hierarchical Macro-Mesoporous Silica

*Liujia Lu,<sup>1</sup> Fei Teng,<sup>2</sup> SenTapas,<sup>3</sup> Dianyu Qi,<sup>1</sup> Lingzhi Wang<sup>\*1</sup> and Jinlong Zhang<sup>\*1</sup>*

<sup>1</sup> Key Laboratory for Advanced Materials and Institute of Fine Chemicals, East China University  
of Science and Technology, 130 Meilong Road, Shanghai 200237, P. R. China

<sup>2</sup> Innovative Research Laboratory of Environment & Energy, Jiangsu Key Laboratory of  
Atmospheric Environment Monitoring & Pollution Control, School of Environmental Science  
and Engineering, Nanjing University of Information Science & Technology

<sup>3</sup> Centre for Materials Science, Institute of Nanotechnology and Bioengineering, School of  
Forensic and Investigative Sciences, University of Central Lancashire, Preston, UK

**ABSTRACT:** Hierarchical macro-mesoporous silica materials co-incorporated with Cr and Ti (MM-Si-Cr-Ti) were directly synthesized by adopting close-packed array of polystyrene microsphere as hard template for macropore through a simple soaking-calcination way, where the Si/Ti ratio was fixed at 200 and Si/Cr ratio varied from 200-10. Ti specie is highly dispersed in the porous matrix and Cr specie mainly exists as tetra-coordinated  $\text{CrO}_3$  when  $\text{Si/Cr} \geq 50$ , and transformed to a mixture of  $\text{CrO}_3$  and crystallized hexa-coordinated  $\text{Cr}_2\text{O}_3$  as determined by

1 wide-angle XRD patterns, raman, EPR spectra and UV-Vis diffuse reflectance spectra. This  
2 highly interconnected porous material co-incorporated with Cr and Ti presented visible-light  
3 driven photocatalytic activity towards the degradation of AO7, which can be optimized by  
4 simply tuning Cr content in the precursor solution. The superiority of hierarchical macro-  
5 mesoporous structure of MM-Si-Cr-Ti over macroporous Si-Cr-Ti oxide (Ma-Si-Cr-Ti) and  
6 mesopores (Me-Si-Cr-Ti) for the photocatalytic application was illustrated by a comparative  
7 study. The visible light responsive activity is attributed to the effective metal to metal charge  
8 transfer from Cr (VI) to Ti (IV), which is benefitted from the uniform dispersion of these two  
9 species in the hierarchical porous matrix.

10 **Keywords:** Hierarchical macro-mesoporous silica; Co-incorporated; visible-light catalytic

## 11 1. INTRODUCTION

12 Recently, hierarchically porous materials with interconnecting binary pore structures have  
13 been widely used for energy conversion[1], sensor devices[2, 3], separation[4], and catalysis[5]  
14 since they combine advantages of pore sizes over different length scales[6-11]. Among them,  
15 inverse opal macroporous-mesoporous structures with macroporous window and mesoporous  
16 skeleton have attracted more attention due to their uniformly arranged macroporous voids, which  
17 often leads to unique performance on photonic modulation and mass transfer[5, 12]. Generally,  
18 hierarchically porous materials composed of macroporous and mesoporous system are  
19 synthesized through a dual-template system using colloidal particle with uniform size as hard  
20 template for macropore and long-chain surfactant as soft template for mesopore[13-15]. Silica  
21 and polymer microspheres including polystyrene (PS) and poly(methyl methacrylate) (PMMA)  
22 are often adopted as hard templates[16-20], which generally assemble into a uniform and close-

1 packed array before the casting of mesoporous precursor through a dip-coating or spin-coating  
2 method. A macroporous-mesoporous inverse opal can be obtained after the removal of hard  
3 template through a dissolution or calcination way.

4 The macropore and mesopore sizes can be largely tuned by adopting appropriate hard and soft  
5 templates[21, 22]. Together with the highly interconnected and accessible pore structure,  
6 hierarchically macroporous-mesoporous materials have attracted considerable attention from the  
7 field of catalysis[23]. Recently, inverse opal mesoporous materials have been successfully  
8 applied for the fabrication of photocatalyst[24, 25]. For examples, hierarchical photocatalysts  
9 with different components such as  $\text{TiO}_2$ ,  $\text{WO}_3$  and  $\text{Bi}_2\text{WO}_6$  have been reported[26-28]. Among  
10 them, silica based hierarchical photocatalyst loaded with highly dispersed semiconductor  
11 nanoparticle or nanocluster have drawn increasingly attention due to its more ordered pore  
12 structure and larger specific surface area than its metal oxide counterparts[29]. When loaded on  
13 matrix with large specific surface area, the agglomeration of nano-photocatalyst can be  
14 effectively inhibited, which is beneficial to the photocatalytic activity due to the more easily  
15 separable photo-generated electron-hole pair[30, 31]. However, this advantage is actually  
16 achieved at the expense of light-absorption range of photocatalyst. For example, the high  
17 dispersion of Ti species in the silica framework increases the splitting degree of energy level,  
18 leading to the widening of the forbidden band and the blue-shift of absorption spectrum[32]. In  
19 order to enhance the visible light absorption ability, some transition metal (V, Mo, Cr etc) was  
20 incorporated into the framework of mesoporous silica besides Ti or  $\text{TiO}_2$ [33, 34]. The pioneering  
21 works observed the activation of synergistic effect of two or more metal which incorporated into  
22 silica. For examples, Guo[35] and Shiraishi[36] et al. reported co-introduced Cr and Ti species  
23 into silica and achieved visible light driven photocatalytic activity from the metal-to-metal

charge-transfer excitation of oxo-bridged bimetallic charge-transfer units (Cr-O-Ti). Kazuhito Hashimoto[37] introduced the photocatalysis driven by the visible light induced hetero-bimetallic Ti(IV)-O-Ce(III) assemblies on the pore of mesoporous silica.

Herein, we adopted inverse opal mesoporous silica as the matrix and simultaneously introduced Ti and Cr to fabricate a visible-light responsive photocatalyst. Inverse opal mesoporous silica is chosen in consideration of its highly interconnected hierarchical pore structure as mentioned above, which should be beneficial to the loading of photocatalyst and the access of pollutant to it. In this paper, the influences of macroporous structure and the existing form of Cr species to the photocatalytic activity were specifically studied. The mechanism was finally proposed based on a systematically comparative study.

## **2. EXPERIMENTAL SECTION**

2.1. Fabrication of different Si-Cr-Ti photocatalysts. Monodisperse PS spheres and the PS photonic crystals were synthesized as described previously[38]. For the preparation of MM-Si-Cr-Ti, 2.2 mL tetraethylorthosilicate (TEOS), 17 mg tetrabutyl titanate (TBOT) and 2.5 mg acetylacetone (AcAc) were mixed together for 30 min (the molar ratios of TBOT/AcAc=2/1). At the same time, 1.0 g F127, 0.1 mL HCl (2 M/L) and 0.8 mL deionized water were dissolved in 16 mL ethanol at 40 °C. After stirring at 25 °C for 1 h, 0.04 g (0.08 g, 0.2 g and 0.4 g)  $\text{Cr}(\text{NO}_3)_3 \cdot 9\text{H}_2\text{O}$  was added and then the mixture was continuously stirred until the solution was clear. To it, the mixtures of TEOS, TBOT and AcAc were added and then the mixture was continuously stirred at 60 °C for 1 h. The molar ratios of Si/Cr/Ti are 200/(2, 4, 10 and 20)/1. Afterwards the PS photonic crystals were immersed into the mesoporous precursor solution. The samples were left to air dry overnight at 25 °C, and were then calcined under air flow to remove the templates, leading to the formation of MM-Si-Cr-Ti. The calcination temperature was

increased from 25 °C to 500 °C with a ramp of 2 °C/min and maintained at 500 °C for 4 h. For comparison, Me-Si-Cr-Ti and Ma-Si-Cr-Ti samples were synthesized according to the above procedure without PS photonic crystals or F127 templates.

On the other hand, TiO<sub>2</sub>/MM-Si-Cr was prepared by introducing Ti species into MM-Si-Cr with a post treatment method. Specifically, MM-Si-Cr was first fabricated using the procedure for MM-Si-Cr-Ti except the absence of TBOT and AcAc in the precursor solution. Subsequently, TBOT and AcAc were dissolved in 10 mL ethanol at 25 °C for 15 min. MM-Si-Cr powders was dispersed in the solution and continuously stirred at 25 °C for 2 h. After the evaporation of ethanol, the samples were then heated at a speed of 2 °C/min to 500 °C and held at this temperature for 4 h. The molar ratio of Ti/Si in the precursor solution for the preparation of TiO<sub>2</sub>/MM-Si-Cr was equal to that of MM-Si-Cr-Ti.

2.2. Characterization. X-ray diffraction (XRD) patterns of the samples were recorded on a Rigaku D/MAX-2550 diffractometer using Cu K $\alpha$  radiation of wavelength 1.5406 Å, typically run at a voltage of 40 kV and current of 100 mA. UV–visible absorbance spectra were achieved for the drypressed disk samples using a Scan UV–visible spectrophotometer (Varian, Cary 500) equipped with an integrating sphere assembly, using BaSO<sub>4</sub> as a reflectance sample. Scanning electron microscopy (SEM) images were obtained with a JEOL JSM-6360LV microscope at an accelerating voltage of 15 kV. Transmission electron microscopy (TEM) images were collected on a JEOL JEM 2010F, electron microscope operated at an acceleration voltage of 200 kV. By utilizing the Barrett–Joyner–Halenda (BJH) model, the pore volumes and pore size distributions were got from the adsorption branches of isotherms. Electron paramagnetic resonance (EPR) spectra were recorded on Varian E-112 at 77K. Catalyst (50 mg) was placed in a quartz EPR tube

and placed on the EPR sample cavity after photoirradiated 20 min using 300 W xenon lamp at  $\lambda > 400$  nm (with filter).

2.3. Photocatalytic Testing. Typically, 40 mg catalyst was added to an aqueous suspension of AO7 (40 mL, 10 mg/L) in a glass tube with vigorously magnetic stirring. The illuminated light source comes from a 300 W xenon lamp which equipped cutoff filter to ensure the wavelengths more than 420 nm. Every hour the above suspension (about 5 mL) was extracted from the mixture solution during visible-light irradiation. The change of concentration of AO7 was tested by the Cary 100 UV-vis spectrometer.

### 3. RESULTS AND DISCUSSION

3.1. Structure and composition of MM-Si-Cr-Ti. The hierarchical porous silica co-incorporated with Cr and Ti was obtained by a method simply combining soaking and calcination treatment, where the washing and centrifugation procedures were avoided. Such a synthesis system is advantageous to the minimization of material loss generally found in other synthesis system. Table 1 shows the actual composition of different MM-Si-Cr-Ti samples analyzed by ICP-AES. It can be found that the actual contents of Cr and Ti species are accordant with their initial concentrations in precursor solutions, which indicates that the preparation method presented here is actually effective to avoid material loss.

Figure 1a shows the close-packed PS array fabricated through a vertical deposition method. An interconnecting macroporous network was formed through a soaking-calcination process as seen from Figure 1b, where the size of the macropore is well accordant with that of PS. This result indicates that the diameter of the macropores can be well controlled by adopting PS particle with different sizes. From the TEM images (Figure 1c-d), interconnected mesopores are clearly observed from the wall of the macropore system. Such a highly interconnected and open

hierarchical porous system makes MM-Si-Cr-Ti excellent carrier for the dispersion of guest molecules. In addition, the BET surface area of MM-Si-Cr-Ti is  $255 \text{ m}^2/\text{g}$ , and the pore volume is  $0.31 \text{ cm}^3/\text{g}$ , which are much bigger than the Ma-Si-Cr-Ti samples and similar to the Me-Si-Cr-Ti samples (Table 2).

The formation of mesoporous structure was further confirmed by low-angle XRD patterns and  $\text{N}_2$  adsorption-desorption isotherms (Fig 2a-b). In Fig 2a, all of samples show a broad diffraction peak attributed to mesoporous characteristics except for the sample prepared at Si/Cr=10, which indicates the high concentration of Cr in the synthesis system has severe interruption effect on the formation of mesoporous structure[39, 40].  $\text{N}_2$  sorption isotherms in Fig 2b display typical type-IV curves with distinct jump between  $P/P_0=0.4-0.7$ , further verifying the mesoporous characteristics.

Fig 3 illustrates the diffuse reflectance UV-vis spectra of MM-Si-Cr samples (Fig 3a) and MM-Si-Cr-Ti samples (Fig 3b). No obvious absorption is observed for pure siliceous sample, while UV bands at 280 nm and 370 nm are found in Cr-incorporated samples, which are usually assigned as  $\text{O} \rightarrow \text{Cr (VI)}$  charge transfer of chromate species in tetrahedral coordination[41]. A weak shoulder peak around 440nm can be assigned to Cr (VI) polychromate[42]. Moreover, it can be found that peak between 600-700 nm attributed to d-d transition of octahedral Cr (III) gradually increases with the decreasing Si/Cr ratio, indicating the formation of  $\text{Cr}_2\text{O}_3$  nanocluster in the pore channel at lower Si/Cr ratio[11, 41, 43]. A comparison between MM-Si-Cr-Ti and MM-Si-Cr samples indicates a new peak appears at about 250 nm, which is obviously much shorter than the maximum absorption wavelength of  $\text{TiO}_2$  nanocrystallite and can be assigned to the ligand-to-metal charge transfer (LMCT) absorption of highly dispersed Ti species[44, 45]. No peak attributed to  $\text{TiO}_2$  crystallite is found from the wide-angle XRD patterns of MM-Si-Cr-



Ti samples (Fig 3d) prepared with different Si/Cr ratios, which only shows increased peak intensity of  $\text{Cr}_2\text{O}_3$  nanocrystal. Raman spectrum is further used to detect the actual state of Ti species. Fig 3c shows the raman spectra of the dehydrated MM-Si-Cr-Ti and MM-Si-Cr samples. The broad Raman band at  $1080\text{ cm}^{-1}$  appears in the MM-Si-Cr-Ti samples can be assigned to silica vibrations perturbed by the presence of Ti, which indicates the existence of the Si–O–Ti bonds[46]. Moreover, there is no band ascribed to rutile or anatase phase, which further excludes the presence of  $\text{TiO}_2$  clusters. These results indicate that MM-Si-Cr-Ti samples prepared through a one-pot way can actually form highly dispersed Cr (VI) and Ti(IV) oxide species by choosing appropriate Si/Cr ratio.

To further confirm the Cr-O-Ti structure and interaction, the properties of chromate species on the catalysts were studied by EPR analysis. The signals at  $g_{\perp}=1.975$  and  $g_{\parallel}=1.952$  were assigned to reduced  $\text{Cr}^{5+}$  from  $\text{Cr}^{6+}$  due to vacuo treatment before EPR analysis (Fig. 4).[47]. After the photoirradiation, the photoinduced electron transfer from  $\text{O}^{2-}$  to  $\text{Cr}^{5+}$  leads to the formation of excited  $\text{Cr}^{4+}$ , so the signal intensity of  $\text{Cr}^{5+}$  was decreased. Compared with that of MM-Si-Cr (Fig. 4a), the intensity of  $\text{Cr}^{5+}$  in MM-Si-Cr-Ti (Fig. 4b) reduces more significantly, indicating the interaction between Cr and Ti. Similar findings have been reported from an oxo-bridged Cr-O-Ti species due to the charge transfer  $\text{Ti}^{4+}$  to  $\text{Cr}^{5+}$  through bridging oxygen, leading to the formation of excited  $\text{Cr}^{4+}\text{-O-Ti}^{3+}$ [36, 48].

3.2. Catalytic Activity. The photocatalytic activity of MM-Si-Cr-Ti samples for the degradation of AO7 was studied under visible-light irradiation (Fig 5a). It is obvious that sample only doped with Ti specie shows negligible visible-light responsive activity due to the wide forbidden band of titanium oxide. However, the activity is significantly improved when only tiny amount of Cr species is introduced for sample prepared at a high Si/Cr ratio of 100. The photocatalytic activity

1 further increases with the decreasing Si/Cr ratio from 100 to 20. However, it cannot be further  
2 improved when the Si/Cr ratio continuously decreases to 10. Moreover, all of samples MM-Si-Cr  
3 only with Cr species show much lower visible-light driven photocatalytic activity than those of  
4 MM-Si-Cr-Ti with tiny Ti besides Cr species (Fig 5b). Therefore, the visible-light driven  
5 photocatalytic activity of samples MM-Si-Cr-Ti co-incorporated with Cr and Ti should be  
6 originated from the visible light absorption ability of Cr species and the subsequent interaction  
7 between Cr and Ti. It is found from the UV-Vis spectra that Cr species is highly dispersed in  
8 silica matrix as isolated Cr (VI) at a low Cr content (Si/Cr=100), which means the visible-light  
9 driven activity is actually initiated from cooperative action between Cr (VI) and Ti (IV) known  
10 as metal to metal charge transfer[37] (MMCT). The decreasing of Si/Cr ratio from 100 to 20  
11 gradually leads to the increasing of Cr content mainly in the forms of oligomeric Cr (VI),  
12 resulting in the further improved photocatalytic activity. The appearance of Cr (III) with the  
13 decreasing Si/Cr ratio indicates a higher polymerization degree of Cr species, which ultimately  
14 leads to the formation of Cr<sub>2</sub>O<sub>3</sub> nanocluster. The formation of Cr<sub>2</sub>O<sub>3</sub> can effectively extend the  
15 light absorption range of the composite to 700 nm. Although the highly dispersed Ti species in  
16 MM-Si-Cr-Ti have a widened forbidden band as verified by its blue shifted maximum absorption  
17 wavelength in UV-Vis spectra compared with TiO<sub>2</sub> nanocrystal. It cannot be excluded that the  
18 excited Cr<sub>2</sub>O<sub>3</sub> cluster may donate electron to the neighboring TiO<sub>2</sub> according to their energy  
19 level of conduction band. However, the formation of Cr<sub>2</sub>O<sub>3</sub> leads to the severe deterioration of  
20 pore structure as found from the small-angle XRD pattern, which makes the effect of Cr<sub>2</sub>O<sub>3</sub> on  
21 the photocatalytic efficiency ambiguous. The pore blockage caused by the formation of Cr<sub>2</sub>O<sub>3</sub>  
22 cluster is definitely disadvantageous to the photocatalytic application. The actual photocatalytic  
23 activity seems to be decreased instead of being improved. Therefore, no matter what is the

possible interaction between  $\text{Cr}_2\text{O}_3$  and  $\text{TiO}_2$ , the pore blockage caused by the formation of  $\text{Cr}_2\text{O}_3$  has a dominant interruption effect on the photocatalytic efficiency. In addition, for the recycling study, the catalyst almost maintains the initial photoactivity after 4 cycles (Fig 6). These results indicate that the MM-Si-Cr-Ti catalyst is stable and can be reused.

Subsequently, the photocatalytic activity of Si-Cr-Ti samples with different porous structure was compared. As shown in Fig 7a, MM-Si-Cr-Ti materials exhibit higher catalytic activities than Ma-Si-Cr-Ti or Me-Si-Cr-Ti samples only with macroporous or mesoporous structure, and the photodegradation of AO7 follows first-order kinetics as shown in Fig 7 (b, c and d), the rate constant on the MM-Si-Cr-Ti is much higher than that on Me-Si-Cr-Ti and Ma-Si-Cr-Ti, which can be explained as follows. MM-Si-Cr-Ti materials have interconnecting binary porestructures, so they combine advantages of pore sizes over different length scales. From the  $\text{N}_2$  adsorption/desorption results (Table 2), it can be clearly seen that the MM-Si-Cr-Ti catalysts have higher specific surface areas and larger pore volume, this hierarchically porous framework is beneficial to adsorption and diffusion of guest species[14], so the pore blockage can be effectively avoided whether for the introduction of metal species or for photocatalytic application. What's more, the ordered macroporous structure gives rise to the photonic stop band for certain frequencies of light[49, 50], so the light absorbance of the catalysts can be promoted due to slow light effect. Hence, MM-Si-Cr-Ti materials have superior advantages for photocatalytic application over traditional mesoporous materials or macroporous materials.

Fig.8 shows the visible-light driven photocatalytic activity (Fig.8a) and the first-order kinetics(Fig. 8b) of MM-Si-Cr-Ti catalysts compared with  $\text{TiO}_2/\text{MM-Si-Cr}$ , where Ti species is introduced through a post treatment method[51]. It is obvious that MM-Si-Cr-Ti shows higher activity than  $\text{TiO}_2/\text{MM-Si-Cr}$ . As mentioned above, the visible-light driven photocatalytic

activity of sample MM-Si-Cr-Ti should be attributed to the metal-metal charge transfer of oxo bridge Cr (VI)-O-Ti (IV) in the framework of MM-Si-Cr-Ti, where the effective coordination between Cr and Ti is essential. Therefore, the decreased activity of sample TiO<sub>2</sub>/MM-Si-Cr should be attributed to the inefficient interaction between Ti and Cr. It is possible that the loading of Ti species through a post treatment results in the formation of Ti species less dispersed, making its contact with Cr oxides less efficient and the decrease of the visible-light responsive activity.

Moreover, the photocatalytic activity of MM-Si-Cr-Ti samples for the degradation of AO7 under UV irradiation was also investigated (Fig. 9). Compared with the results from visible light irradiation, it is found that the catalysts show poorer UV-light driven activities, which seems not much influenced by the increasing content of Cr. The results well illustrate that Ti species plays a dominant role in the UV-light irradiated photocatalysis, while oxo-bridged Cr-O-Ti species is the key factors for visible-light irradiated photocatalysis.

#### 4. CONCLUSIONS

In summary, we demonstrated a simple soaking-calcination method to synthesize hierarchical macro-mesoporous silica based photocatalyst co-incorporated with Cr and Ti (MM-Si-Cr-Ti), which show cooperative effect for the visible light responsive activity towards the degradation of AO7. The highly interconnected and accessible porous structure and the effective interaction between uniformly dispersed Cr (VI) and Ti (IV) species make MM-Si-Cr-Ti more highly active under visible light irradiation than macroporous Ma-Si-Cr-Ti, mesoporous Me-Si-Cr-Ti and TiO<sub>2</sub>/MM-Si-Cr with less dispersed Ti species.

#### AUTHOR INFORMATION

#### Corresponding Author

\*E-mail: jlzhang@ecust.edu.cn. wlz@ecust.edu.cn

Notes

The authors declare no competing financial interest.

#### ACKNOWLEDGMENT

This work has been supported by the National Nature Science Foundation of China (21173077, and 21237003); the National Basic Research Program of China (973 Program, 2013CB632403); the Project of International Cooperation of the Ministry of Science and Technology of China (No.2011DFA50530); Science and Technology Commission of Shanghai Municipality (12230705000, 12XD1402200); the Research Fund for the Doctoral Program of Higher Education (20120074130001); Open Project from Jiangsu Key Laboratory of Atmospheric Environment Monitoring and Pollution Control of Nanjing University of Information Science and Technology (kHK1110), Jiangsu Province Innovation Platform for Superiority Subject of Environmental Science and Engineering.

#### REFERENCES

[1] C.M. Doherty, R.A. Caruso, B.M. Smarsly, C.J. Drummond, Chem. Mater., 21 (2009) 2895-2903.

[2] Y.J. Lee, C.E. Heitzman, W.R. Frei, H.T. Johnson, P.V. Braun, J. Phys. Chem. B, 110 (2006) 19300-19306.

[3] R.A. Barry, P. Wiltzius, Langmuir, 22 (2005) 1369-1374.

[4] K. Nakanishi, N. Tanaka, Acc. Chem. Res., 40 (2007) 863-873.

- 1 [5] J. Zhao, F. Cheng, C. Yi, J. Liang, Z. Tao, J. Chen, J. Mater. Chem., 19 (2009) 4108-4116.
- 2 [6] K. Kanamori, K. Nakanishi, Chem. Soc. Rev., 40 (2011) 754-770.
- 3 [7] Z. Sun, Y. Deng, J. Wei, D. Gu, B. Tu, D. Zhao, Chem. Mater., 23 (2011) 2176-2184.
- 4 [8] G.L. Drisko, M. Chee Kimling, N. Scales, A. Ide, E. Sizgek, R.A. Caruso, V. Luca,  
5 Langmuir, 26 (2010) 17581-17588.
- 6 [9] A. Lemaire, B.-L. Su, Langmuir, 26 (2010) 17603-17616.
- 7 [10] T.Y. Ma, Z.Y. Yuan, Eur. J. Inorg. Chem., 2010 (2010) 2941-2948.
- 8 [11] B.M. Weckhuysen, L.M. De Ridder, R.A. Schoonheydt, J. Phys. Chem, 97 (1993) 4756-  
9 4763.
- 10 [12] J. Lei, L. Wang, J. Zhang, ACS Nano, 5 (2011) 3447-3455.
- 11 [13] Y. Deng, C. Liu, T. Yu, F. Liu, F. Zhang, Y. Wan, L. Zhang, C. Wang, B. Tu, P.A. Webley,  
12 H. Wang, D. Zhao, Chem. Mater., 19 (2007) 3271-3277.
- 13 [14] M. Xu, D. Feng, R. Dai, H. Wu, D. Zhao, G. Zheng, Nanoscale, 3 (2011) 3329-3333.
- 14 [15] L. Samiee, A. Beitollahi, Res. Chem. Intermed., (2013) 1-17.
- 15 [16] O.D. Velev, T.A. Jede, R.F. Lobo, A.M. Lenhoff, Nature, 389 (1997) 447-448.
- 16 [17] A. van Blaaderen, Science, 282 (1998) 887-888.
- 17 [18] J.E.G.J. Wijnhoven, S.J.M. Zevenhuizen, M.A. Hendriks, D. Vanmaekelbergh, J.J. Kelly,  
18 W.L. Vos, Adv. Mater., 12 (2000) 888-890.

- 1 [19] J.D. Joannopoulos, *Nature*, 414 (2001) 257-258.
- 2 [20] T. Kamegawa, N. Suzuki, H. Yamashita, *Chem. Lett.*, 38 (2009) 610-611.
- 3 [21] Y. Liu, L. Wang, J. Zhang, F. Chen, M. Anpo, *Res. Chem. Intermed.*, 37 (2011) 949-959.
- 4 [22] Y. Wang, G. Chen, F. Zhang, L. Li, *Res. Chem. Intermed.*, 40 (2014) 385-397.
- 5 [23] T. Yan, L. Li, G. Li, *Res. Chem. Intermed.*, 37 (2011) 297-307.
- 6 [24] J.G. Yu, Y.R. Su, B. Cheng, *Adv. Funct. Mater.*, 17 (2007) 1984-1990.
- 7 [25] F. Lu, W. Cai, Y. Zhang, *Adv. Funct. Mater.*, 18 (2008) 1047-1056.
- 8 [26] T. Kamegawa, N. Suzuki, M. Che, H. Yamashita, *Langmuir*, 27 (2011) 2873-2879.
- 9 [27] Z. Gu, T. Zhai, B. Gao, X. Sheng, Y. Wang, H. Fu, Y. Ma, J. Yao, *J. Phys. Chem. B*, 110  
10 (2006) 23829-23836.
- 11 [28] M. Shang, W. Wang, L. Zhang, S. Sun, L. Wang, L. Zhou, *J. Phys. Chem. C*, 113 (2009)  
12 14727-14731.
- 13 [29] E. Mehrasbi, Y. Sarrafi, A. Vahid, H. Alinezhad, *Res. Chem. Intermed.*, (2014) 1-13.
- 14 [30] B.I. Park, H. Jie, B.G. Song, K.M. Kang, J.K. Park, S.H. Cho, *Res. Chem. Intermed.*, 40  
15 (2014) 115-126.
- 16 [31] L. Jiang, L. Wang, J. Zhang, *Chem. Commun.*, 46 (2010) 8067-8069.
- 17 [32] L. Samiee, A. Beitollahi, M. Bahmani, M.M. Akbarnejad, A. Vinu, *Res. Chem. Intermed.*,  
18 36 (2010) 897-923.

- 1 [33] Y. Shao, L. Wang, J. Zhang, M. Anpo, J. Phys. Chem. B, 109 (2005) 20835-20841.
- 2 [34] H. Liu, Y. Wu, J. Zhang, ACS Appl. Mater. Interfaces, 3 (2011) 1757-1764.
- 3 [35] S. Shen, L. Guo, Catal. Today, 129 (2007) 414-420.
- 4 [36] D. Tsukamoto, A. Shiro, Y. Shiraishi, T. Hirai, J. Phys. Chem. C, 115 (2011) 19782-19788.
- 5 [37] R. Nakamura, A. Okamoto, H. Osawa, H. Irie, K. Hashimoto, J. Am. Chem. Soc., 129  
6 (2007) 9596-9597.
- 7 [38] S.E. Shim, Y.J. Cha, J.M. Byun, S. Choe, J. Appl. Polym. Sci., 71 (1999) 2259-2269.
- 8 [39] B. Sun, E.P. Reddy, P.G. Smirniotis, Appl. Catal., B, 57 (2005) 139-149.
- 9 [40] B. Sun, E.P. Reddy, P.G. Smirniotis, J. Catal., 237 (2006) 314-321.
- 10 [41] B.M. Weckhuysen, I.E. Wachs, R.A. Schoonheydt, Chem. Rev., 96 (1996) 3327-3350.
- 11 [42] K. Takehira, Y. Ohishi, T. Shishido, T. Kawabata, K. Takaki, Q. Zhang, Y. Wang, J. Catal.,  
12 224 (2004) 404-416.
- 13 [43] E. Groppo, C. Lamberti, S. Bordiga, G. Spoto, A. Zecchina, Chem. Rev., 105 (2005) 115-  
14 184.
- 15 [44] X. Gao, S.R. Bare, J.L.G. Fierro, M.A. Banares, I.E. Wachs, J. Phys. Chem. B, 102 (1998)  
16 5653-5666.
- 17 [45] S. Bordiga, S. Coluccia, C. Lamberti, L. Marchese, A. Zecchina, F. Boscherini, F. Buffa, F.  
18 Genoni, G. Leofanti, J. Phys. Chem, 98 (1994) 4125-4132.



[46] X. Gao, S.R. Bare, J. Fierro, M.A. Banares, I.E. Wachs, J. Phys. Chem. B, 102 (1998) 5653-5666.

[47] B.M. Weckhuysen, R.A. Schoonheydt, F.E. Mabbs, D. Collison, J. Chem. Soc., Faraday Trans., 92 (1996) 2431-2436.

[48] S. Rodrigues, K.T. Ranjit, S. Uma, I.N. Martyanov, K.J. Klabunde, Adv. Mater., 17 (2005) 2467-2471.

[49] K. Sakoda, Opt. Express, 4 (1999) 167-176.

[50] A. Imhof, W.L. Vos, R. Sprik, A. Lagendijk, Phys. Rev. Lett., 83 (1999) 2942.

[51] L.Z. Wang, L. Jiang, C.C. Xu, J.L. Zhang, J. Phys. Chem. C, 116 (2012) 16454-16460.

## Figure Captions

**Fig.1** SEM (a, b) and TEM (c, d) images of MM-Si-Cr-Ti prepared with molar ratio of Si/Cr/Ti=200/10/1.

**Fig.2** Low-angle XRD patterns (a) and N<sub>2</sub> adsorption/desorption isotherms (b) of MM-Si-Cr-Ti samples with different Si/Cr molar ratios.

**Fig. 3** (a) UV–vis diffuse reflectance spectra of MM-Si-Cr samples; (b) UV–vis diffuse reflectance spectra of MM-Si-Cr-Ti samples; (c) Raman spectra of MM-Si-Cr-Ti and MM-Si-Cr samples, the molar ratio of Si/Cr/Ti=200/2/1; (d) Wide-angle XRD patterns MM-Si-Cr-Ti samples prepared with different Si/Cr molar ratios.

**Fig. 4** EPR spectra (77 K) of (a) MM-Si-Cr and (b) MM-Si-Cr-Ti samples measured without photoirradiation (black) and after photoirradiation (red). The molar ratio of Si/Cr =100/1.

**Fig.5** Photocatalytic activity of different Si/Cr molar ratio MM-Si-Cr-Ti samples (a) and MM-Si-Cr samples (b) for the degradation of AO7 under visible light.

**Fig. 6** Cycling photo-degradation of AO7 under visible-light illumination with MM-Si-Cr-Ti, The molar ratio of Si/Cr =20/1.

**Fig. 7** (a)Visible-light driven photodegradation rate of AO7 with Ma-Si-Cr-Ti, MM-Si-Cr-Ti and Me-Si-Cr-Ti; (b, c and d) Photodegradation kinetics of AO7 under visible light irradiation for MM-Si-Cr-Ti-X, Me-Si-Cr-Ti-X and Ma-Si-Cr-Ti-X, respectively, where X represents the ratios of Si/Cr.

**Fig. 8** (a) Visible-light driven photodegradation rate of AO7 with MM-Si-Cr-Ti and TiO<sub>2</sub>/MM-Si-Cr; (b) Kinetics of AO7 photodegradation under visible light irradiation for MM-Si-Cr-Ti and TiO<sub>2</sub>/MM-Si-Cr, respectively.

**Fig. 9** Photocatalytic activity of MM-Si-Cr-Ti prepared with different Si/Cr molar ratios for the degradation of AO7 under UV irradiation.

**Table. 1** Element weight percentage of MM-Si-Cr-Ti materials

**Table 2. B** Structural and textural parameters of samples Ma-Si-Cr-Ti, MM-Si-Cr-Ti and Me-Si-Cr-Ti.

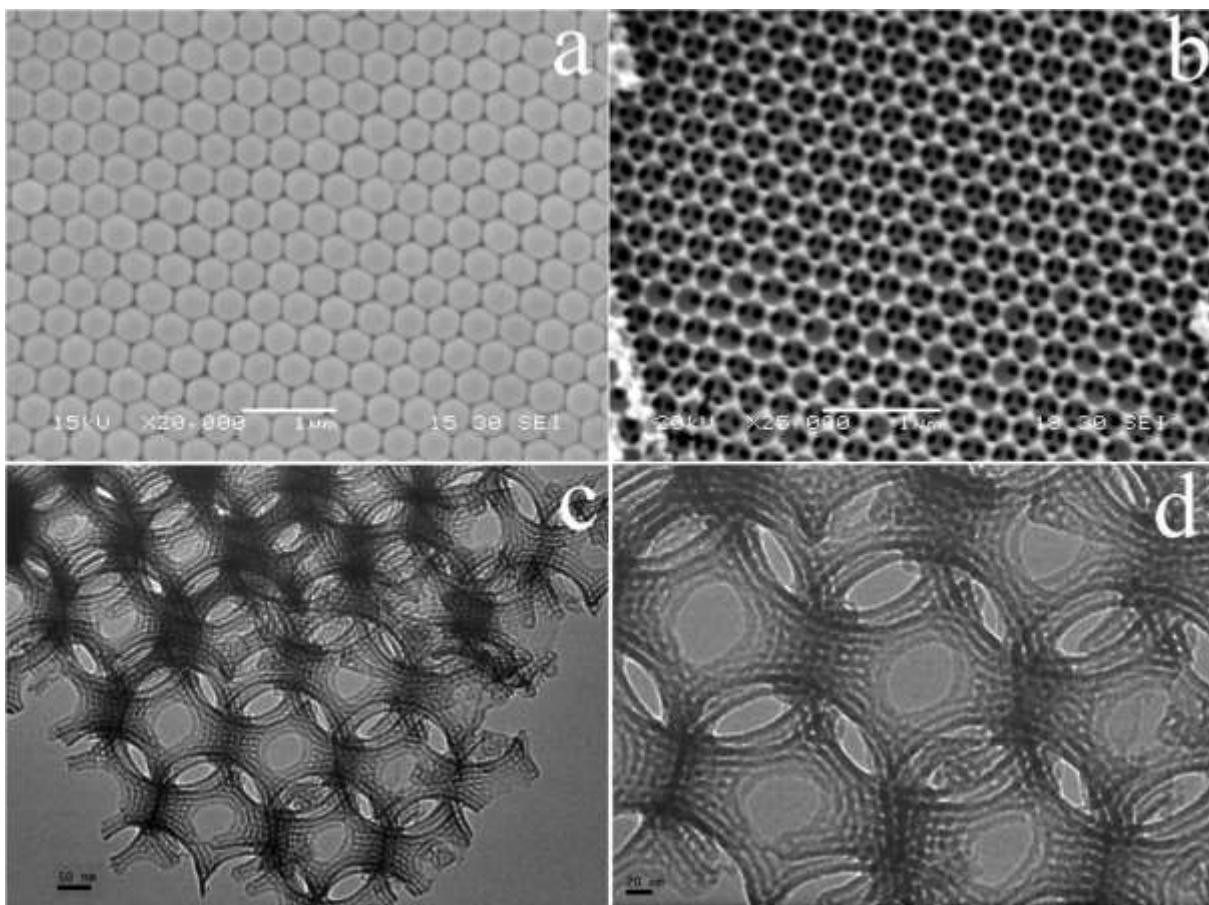


Fig.1

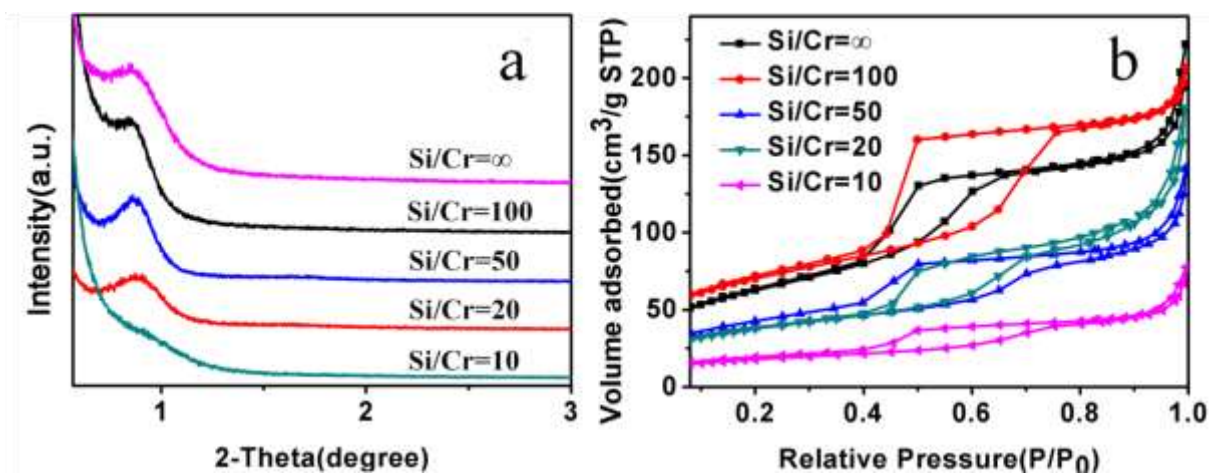


Fig.2

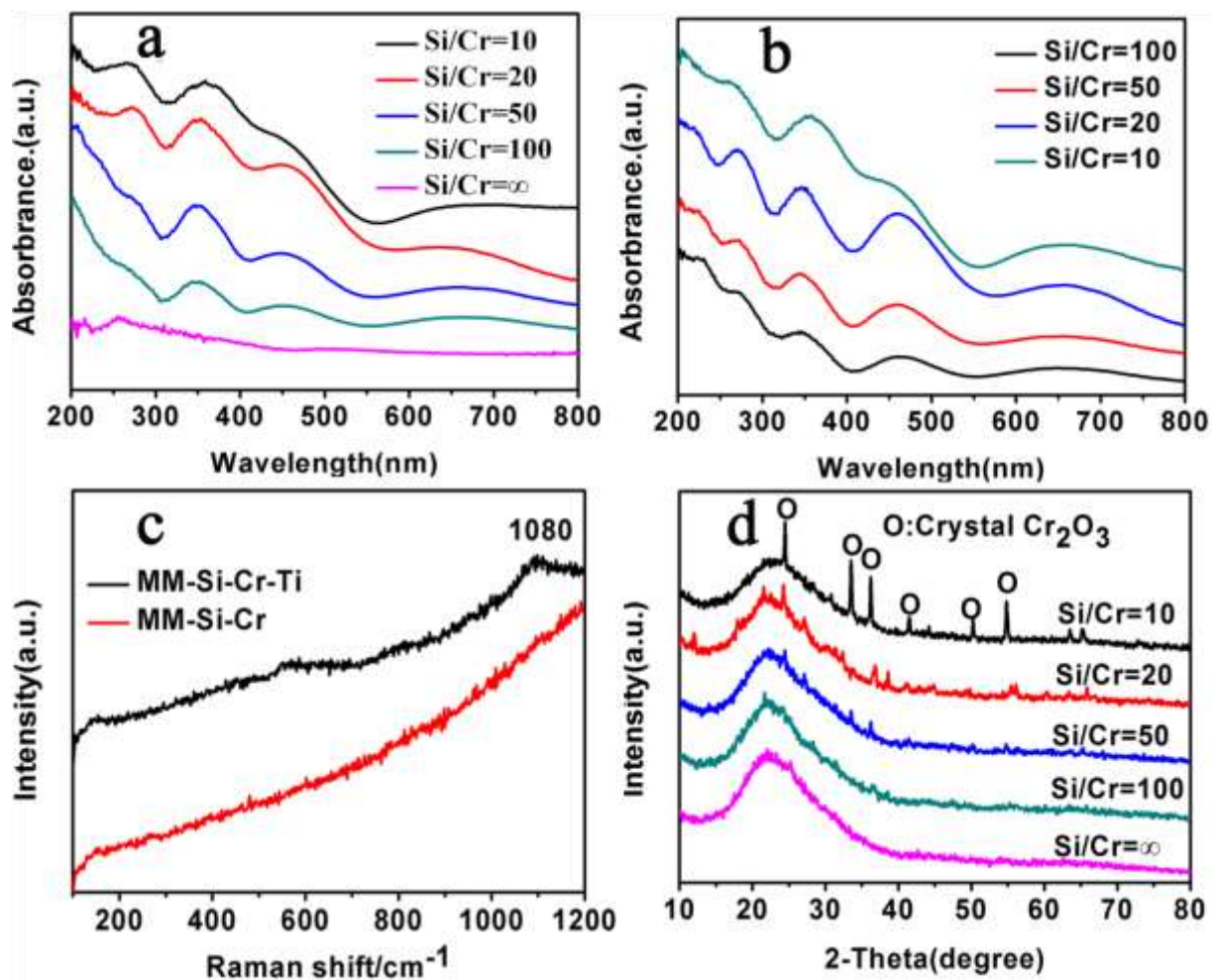


Fig.3

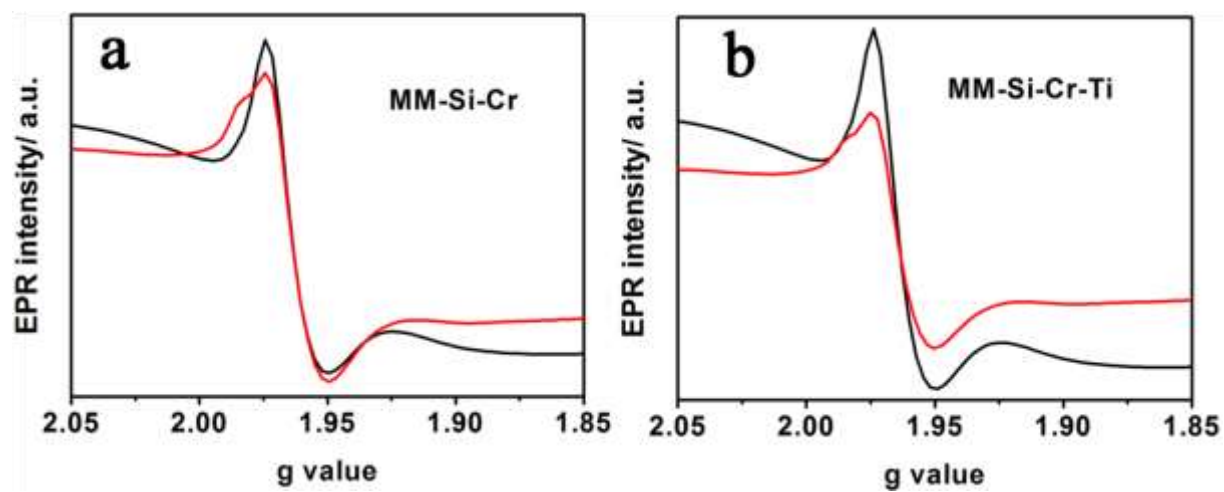


Fig.4

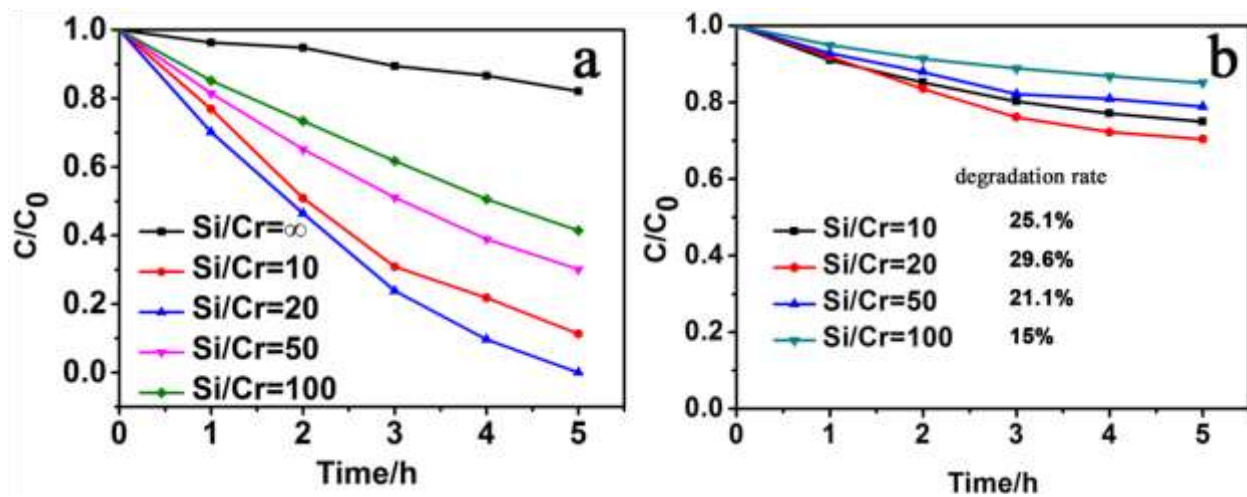


Fig.5

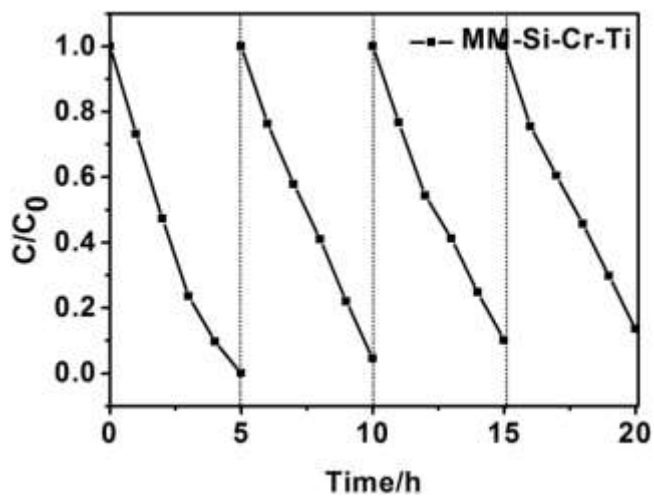


Fig 6



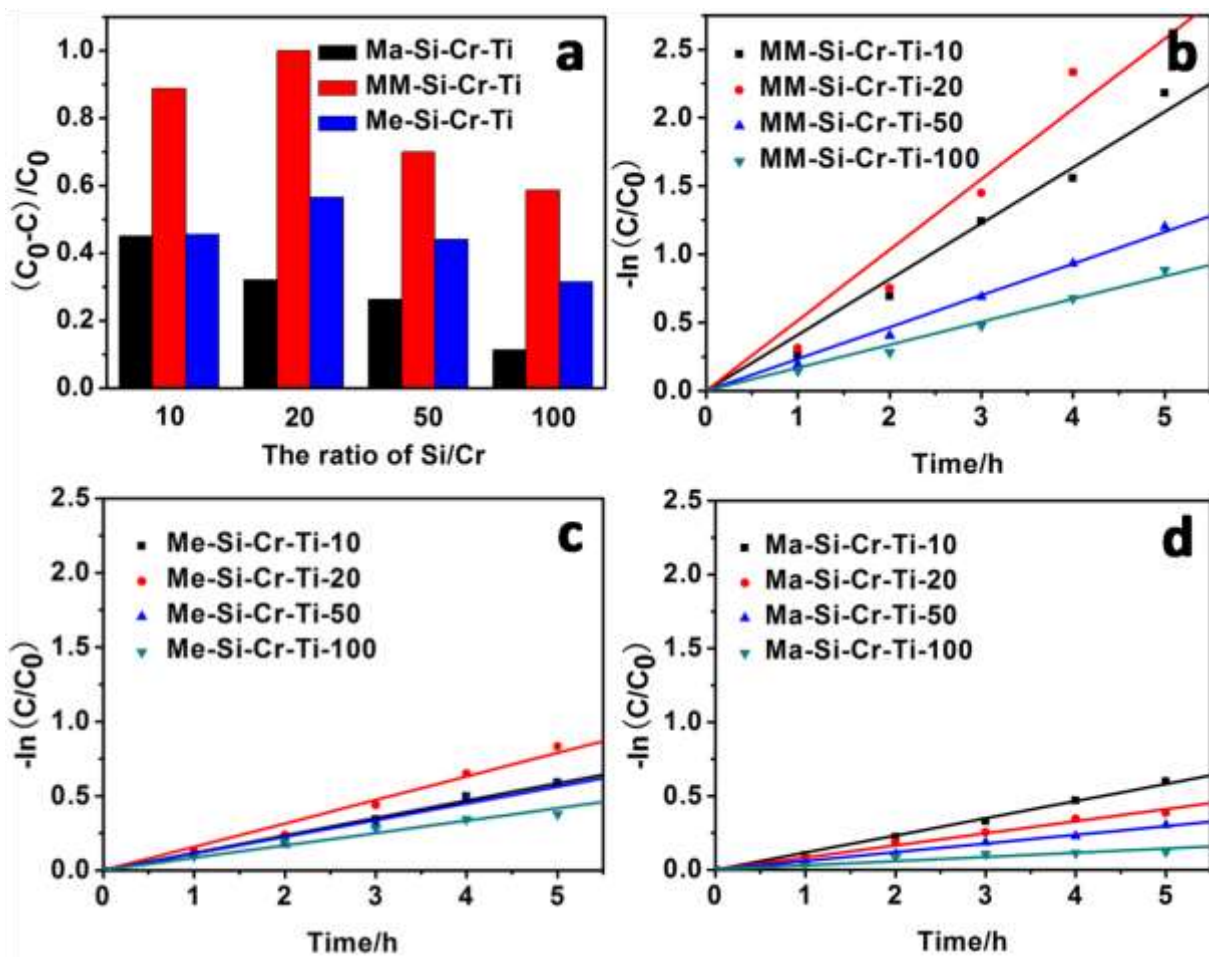


Fig.7

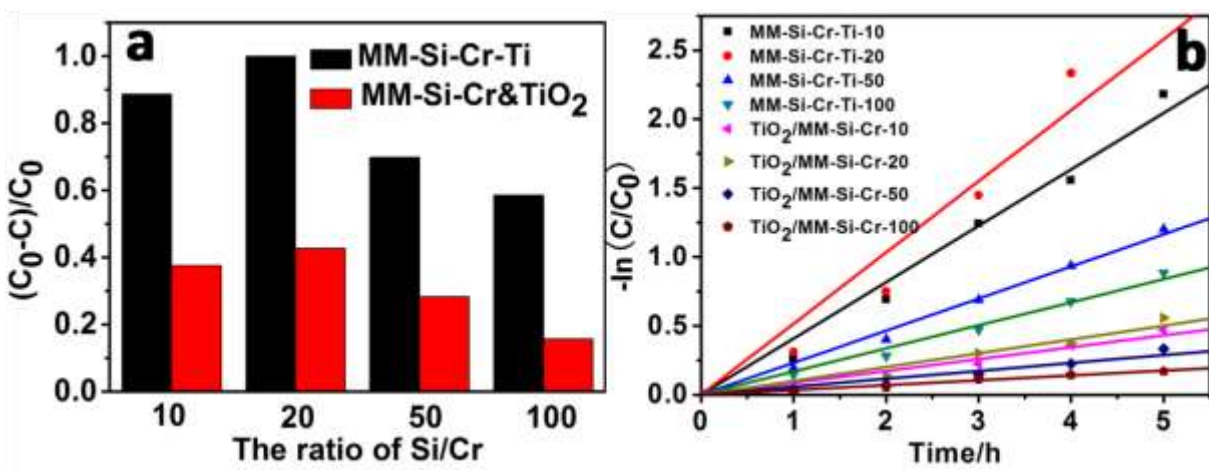
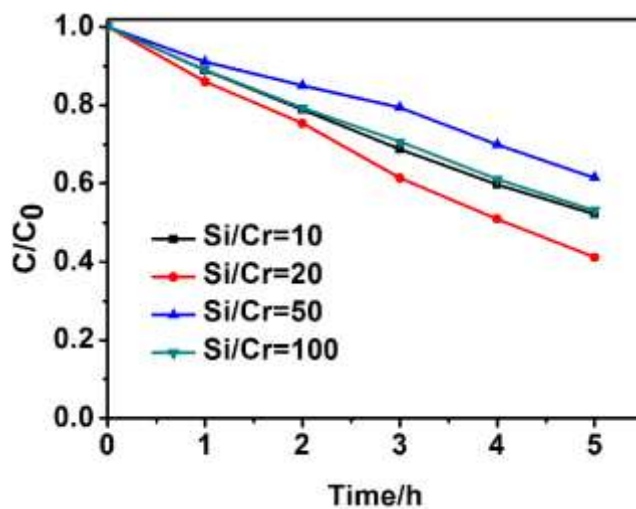


Fig.8



**Fig.9**

**Table.1**

element	O	Si	Cr	Ti	total
Si/Cr =10	45.31	43.70	10.55	0.44	100
Si/Cr =20	44.91	49.92	4.71	0.46	100
Si/Cr =50	44.65	52.73	2.15	0.47	100
Si/Cr =100	44.98	53.43	1.12	0.47	100

**Table.2**

Sample <sup>a</sup>	SBET <sup>b</sup> (m <sup>2</sup> /g)	V <sub>t</sub> <sup>c</sup> (cm <sup>3</sup> /g)	D <sub>pa</sub> <sup>d</sup> (nm)	D <sub>pd</sub> <sup>e</sup> (nm)
Ma-Si-Cr-Ti	74	0.091	---	---
MM-Si-Cr-Ti	255	0.31	5.1	4.6



---

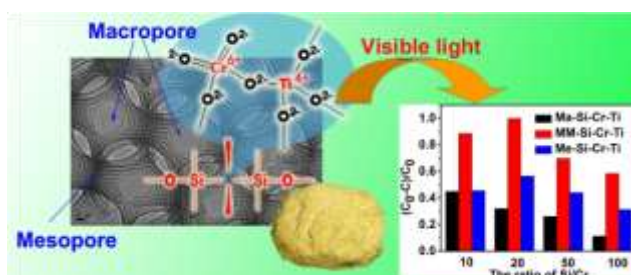
Me-Si-Cr-Ti	280	0.26	4.5	3.7
-------------	-----	------	-----	-----

---

<sup>a</sup> Sample stand for the three different structure of samples with molar ratio of Si/Cr/Ti=200/10/1. <sup>b</sup> SBET is the specific surface area measured from N<sub>2</sub> physisorption. <sup>c</sup> V<sub>t</sub> is the pore volume measured at P/P<sub>0</sub>= 0.99. <sup>d</sup> D<sub>pa</sub> and <sup>e</sup> D<sub>pd</sub> are the pore size were calculated from N<sub>2</sub> sorption isotherm based on BJH model from adsorption and desorption branches, respectively.

---

## Graphic Abstract



Hierarchical macro-mesoporous silica materials co-incorporated with Cr and Ti (MM-Si-Cr-Ti) were directly synthesized using polystyrene arrays as hard templates for macropore, which presented visible-light driven photocatalytic activity towards the degradation of AO7. Compared with samples with only macropores (Ma-Si-Cr-Ti) or mesopores (Me-Si-Cr-Ti), MM-Si-Cr-Ti exhibited higher activity due to the highly interconnected and accessible pore structure. The visible light responsive activity is attributed to the effective metal to metal charge transfer from Cr (VI) to Ti (IV), which is benefitted from the uniform dispersion of these two species and their efficient contact in the porous matrix.

1

2

3

4